Quasi-One-Dimensional Cyano-Phenylene Aggregates

Uniform Molecule Alignment Contrasts Varying Electrostatic Surface Potential

Balzer, Frank; Resel, Roland; Lützen, Arne; Schiek, Manuela

Published in:
The Journal of Chemical Physics

DOI:
10.1063/1.4979484

Publication date:
2017

Document version
Publisher's PDF, also known as Version of record

Citation for pulished version (APA):
Balzer, F., Resel, R., Lützen, A., & Schiek, M. (2017). Quasi-One-Dimensional Cyano-Phenylene Aggregates: Uniform Molecule Alignment Contrasts Varying Electrostatic Surface Potential. The Journal of Chemical Physics, 146(13), [134704]. DOI: 10.1063/1.4979484

Quasi-one-dimensional cyano-phenylene aggregates: Uniform molecule alignment contrasts varying electrostatic surface potential

Frank Balzer, Roland Resel, Arne Lützen, and Manuela Schiek

Citation: The Journal of Chemical Physics **146**, 134704 (2017); doi: 10.1063/1.4979484
View online: http://dx.doi.org/10.1063/1.4979484
View Table of Contents: http://aip.scitation.org/toc/jcp/146/13
Published by the American Institute of Physics

Quasi-one-dimensional cyano-phenylene aggregates: Uniform molecule alignment contrasts varying electrostatic surface potential

Frank Balzer,[1,a)] Roland Resel,[2] Arne Lützen,[3] and Manuela Schiek[4]
[1]*NanoSyd, Mads Clausen Institute, University of Southern Denmark, 6400 Sønderborg, Denmark*
[2]*Institute of Solid State Physics, Graz University of Technology, Petersgasse 16, 8010 Graz, Austria*
[3]*Kekulé-Institute for Organic Chemistry and Biochemistry, University of Bonn, Gerhard-Domagk-Straße 1, 53121 Bonn, Germany*
[4]*Energy and Semiconductor Research Laboratory, Institute of Physics, University of Oldenburg, Carl-von-Ossietzky-Straße 9-11, 26129 Oldenburg, Germany*

(Received 23 February 2017; accepted 17 March 2017; published online 3 April 2017)

The epitaxial growth of the mono-functionalized *para*-quaterphenylene molecule CNHP4 on muscovite mica is investigated. The vacuum deposited molecules aggregate into nanofibers of varying morphology. Due to muscovite's *cm* symmetry, almost mutually parallel fibers grow. Polarized light microscopy together with X-ray diffraction resolves the projected orientation of the molecules on the substrate surface and within the fibers. Several different contact planes with the substrate are detected. For all of them, the molecules orient with their long molecule axis approximately perpendicular to the grooved muscovite direction, so that the alignment of the molecules on the substrate is uniform. Kelvin probe force microscopy finds vastly different electrostatic properties of different fiber types and facets. *Published by AIP Publishing.* [http://dx.doi.org/10.1063/1.4979484]

I. INTRODUCTION

The epitaxial growth of quasi-one-dimensional crystalline aggregates from organic molecules such as *para*-phenylenes,[1–3] naphthyl end-capped oligothiophenes,[4] α-thiophenes,[5,6] or phenylene-thiophene co-oligomers[7,8] has been investigated in detail during the last two decades. This research was driven both by the desire to obtain a better understanding of the underlying, epitaxial growth mechanisms[9] and by the use of these highly anisotropic systems in applications such as waveguides and nanolasers.[10–14] In this context, uniaxial molecular films, fibers, and fiber assemblies have numerous additional applications in, e.g., molecular electronics, sensors, and photonics.[15–17] A specific functionalization of the molecular building blocks can induce targeted optoelectronic and morphological properties.[18,19] The *para*-quaterphenylene molecule p-4P has, e.g., been successfully functionalized in the *para* positions with various electron-pulling and -pushing groups.[20–22] Cyano-functionalization is of special interest due to the strong electron withdrawing effect, resulting in an asymmetric charge distribution, and due to the capability of the CN group to form hydrogen bonds.[23–27] It has thus the potential to impact molecular packing, the electronic structure of crystallite facets, thin film formation, and self-assembly,[28] and hence can convert a p-type organic semiconductor into an n-type one.[29,30] Consequently, optical properties such as the fluorescence quantum yield might be enhanced as well.[31]

Anisotropic substrates such as $TiO_2(1\,1\,0)$[32,33] and Cu(1 1 0),[34,35] friction transferred poly-(tetrafluoroethylene) (PTFE) and polythiophene,[36,37] and nanoporous substrates[38–40] have been used in the past as templates to form uniaxially aligned entities from organic molecules. Here, muscovite mica is used as a model substrate. Due to its *cm* surface symmetry, the deposition of organic molecules often leads to the anisotropic formation of crystallites and fiber-like growth.[41–44] These fibers have been wet-transferred to other surfaces of choice or dispersed in liquids, multiplying their application potential.[45]

Previously, the growth of the symmetrically cyano-functionalized *para*-quaterphenylene (1,4‴-dicyano-4, 1′ : 4′, 1″:4″, 1‴-quaterphenylene, CNP4) on muscovite mica has been evaluated. It has been shown that, although different crystallites with different in-plane orientations form, the projection of the molecules' long axes onto the substrate surface is always perpendicular to the surface mirror plane.[46] In this paper, we investigate the growth of the mono-functionalized quaterphenylene CNHP4, i.e., of 1-cyano-(4 : 1′, 4′ : 1, 4″ : 1‴)-quaterphenylene. The single molecule is rod-like and has a length of 19.6 Å; its chemical structure is depicted as an inset in Figure 1. This molecule possesses a permanent electric dipole moment and a rather large hyperpolarizability.[47,48] CNHP4 nanofibers show second order susceptibility $\chi^{(2)}$ of the order of 2 pm/V.[49,50] It is therefore also of major interest for nonlinear-optical applications such as the use in organic-plasmonic hybrids.[51]

Para-phenylenes without solubilizing side-chains are notoriously difficult to crystallize by conventional solution-assisted methods due to their low solubility.[24] Single crystalline entities from alike molecules have successfully been grown in a vapor phase deposition furnace,[52–54] but not for CNHP4, yet. For thin films from upright standing CNHP4

a)Author to whom correspondence should be addressed. Electronic mail: fbalzer@mci.sdu.dk

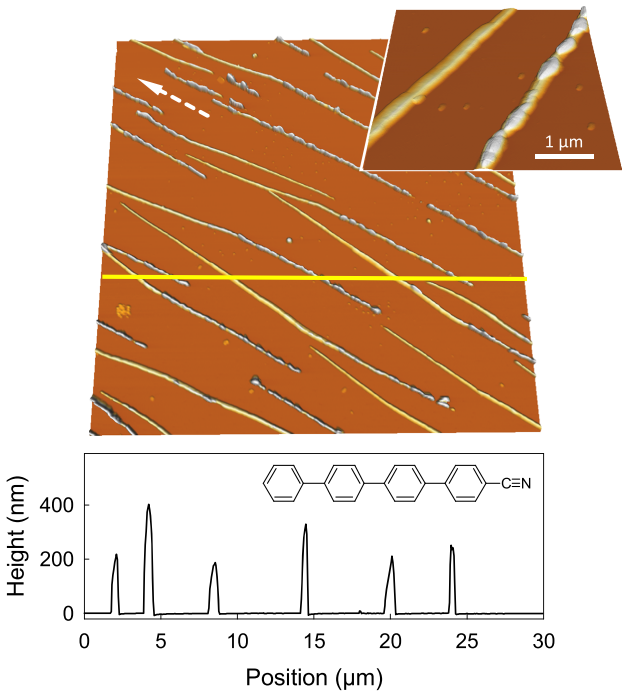

FIG. 1. The three-dimensional view of the AFM image together with a height profile along the yellow solid line visualizes two different CNHP4 nanofiber morphologies. The grooved muscovite $\langle 1\,1\,0\rangle_g$ direction is denoted by a white dashed arrow. The structural formula of 1-cyano-(4 : 1′, 4′ : 1, 4″ : 1‴)-quaterphenylene (CNHP4) and a zoom into the two fiber morphologies are shown as insets.

molecules formed on SiO_x surfaces, the crystal structure has been determined by a combination of X-ray diffraction and *ab initio* calculations from two-dimensional powders.[55,56] Several polymorphs have been detected. One of them was attributed to the bulk phase, where CNHP4 crystallizes into a monoclinic unit cell with cell parameters $a = 5.56(5)$ Å, $b = 7.67(3)$ Å, $c = 20.85(5)$ Å, and $\beta = 97.4° \pm 1°$. The molecules are herringbone packed and stand upright on the (0 0 1) face. The other polymorphs have slightly larger *d*-spacings, but their accurate crystal structures have not been provided.

II. EXPERIMENTAL

Muscovite mica (Structure Probe, Inc., and Plano GmbH) is cleaved in air, mounted onto a sample holder made from oxygen free copper, and transferred into a vacuum chamber within a few 10 s. After pump-down to a base pressure of 1×10^{-8} mbar, it delivers a clear diffraction pattern from a LEED-apparatus[3,57] (Omicron MCP-LEED). During thin film deposition from a home-made Knudsen cell, the pressure rises to about 4×10^{-7} mbar. The substrate can be heated by a filament placed underneath the sample holder. All given temperatures are sample holder temperatures. After molecule deposition, the samples are investigated *in situ* by LEED, and under ambient conditions by atomic force microscopy (AFM) in intermittent contact mode (JPK Nanowizard, BudgetSensors Tap 300, force constant 40 N/m, tip radius smaller than 10 nm). The electrical surface potential is probed by Kelvin probe force microscopy (KPFM, JPK Nanowizard) in hover mode (50 nm hover height). For this, Pt-coated tips are used (AppNano ANSCM-PA with a force constant of 40 N/m and a tip radius 30 nm). For KPFM, the samples are glued with silver paste (Structure Probe, Inc.) to a grounded stainless steel stub. Optical microscopy is conducted by a confocal laser scanning microscope (Olympus LEXT OLS4100 and Keyence VK-X200). Fluorescence microscope images are obtained with a Nikon Eclipse TE-300 epifluorescence microscope equipped with a high-pressure Hg-lamp (excitation wavelength $\lambda_{exc} \approx 365$ nm). For the analysis of the polarization of the emitted fluorescence, the samples are mounted on a computer-controlled rotational stage (Thorlabs PRM1) on the fluorescence microscope table, and the emitted blue light is observed through a sheet polarizer with its transmission axis being perpendicular to the symmetry axis of the microscope to minimize depolarization artifacts. The polarization directions are related to the substrate high symmetry directions, which are determined by means of a percussion figure.[58,59] The muscovite mica (0 0 1) face consists of SiO_4 tetrahedra. Muscovite is a dioctahedral mica, resulting in a tilt of the SiO_4 tetrahedra along one of the two $\langle 1\,1\,0\rangle$ directions,[60] so that sub-nanometer deep grooves are formed. Their direction is denoted by the index "g," and the non-grooved $\langle 1\,1\,0\rangle$ direction by "ng."

Specular X-ray diffraction is performed in the Bragg-Brentano configuration with Cu-Kα radiation ($\lambda = 1.542$ Å). Samples have to be considerably thicker than for the optical and AFM investigations to deliver reliable diffraction peaks. In Figures S1(a) and S1(b) in the supplementary material, fluorescence microscope images from a thin and a thick sample are compared, showing a similar morphology except for a larger number density of fibers. Furthermore, the samples are often wet-transferred to glass to get rid of strong muscovite diffraction peaks. In-plane alignment is determined by means of X-ray pole figures with Cr-Kα radiation at $\lambda = 2.291$ Å. X-ray diffraction pole figures are collected with a PHILIPS X'Pert System equipped with an ATC3 Eulerian cradle. A monochromator at the secondary side is used. Comparison of the experimental data with calculated pole figures is performed with the software STEREOPOLE.[61]

III. RESULTS AND DISCUSSION

Vapor deposition of CNHP4 molecules at elevated temperatures on muscovite mica leads to the formation of nanofibers. They grow approximately along the grooved substrate direction, i.e., along $\langle 1\,1\,0\rangle_g$. An AFM image of the fibers, formed at a substrate temperature of $T_s = 323$ K, is presented in Figure 1. Here, fibers are between 200 nm and 400 nm tall; the nominal thickness of the deposited material is $d = 12$ nm. Two types of morphologies are observed: fibers with an asymmetric, triangular cross section and rather well defined facets, and less well defined entities consisting of bits of different heights and varying widths. They often do not exist separately, but merge into one another. The inset in Figure 1 displays these two types in more detail. Directly after deposition, a large number of small clusters are observed in between the fibers. These clusters mostly vanish on a time scale of days under ambient conditions in contact with atmospheric water vapor due to Ostwald ripening.[62]

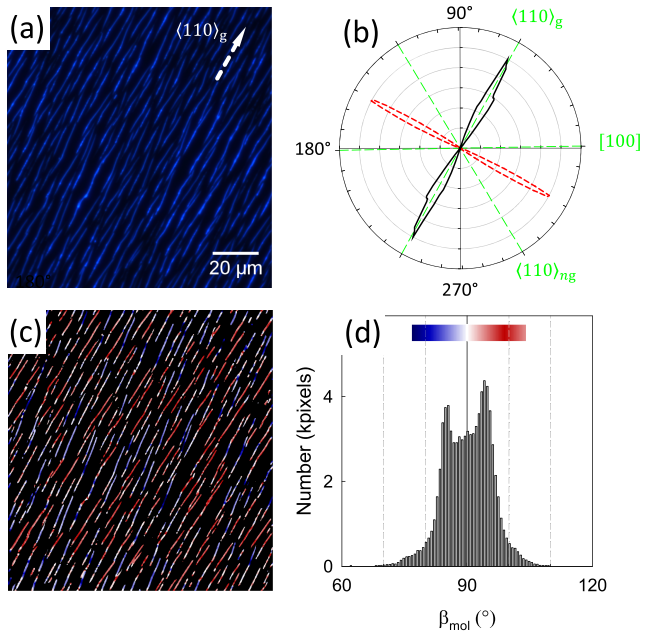

FIG. 2. Fluorescence microscope image (a) of CNHP4 fibers (nominal thickness $d = 12$ nm) grown on muscovite mica at a substrate temperature of 323 K. Muscovite $\langle 1\,1\,0\rangle_g$ is denoted by a dashed white arrow. (b) Distribution of fiber orientations (black solid line) and of polarization angles ϕ_{pol} (red dashed line). The spatially resolved values of molecule orientations β_{mol} within the fibers are superimposed in (c) onto the fluorescence microscope image. The color code is given in (d), where the integrated distribution of β_{mol} shows two maxima at 85° and 95°, respectively.

The diffraction of low energy electrons (LEED) from thin CNHP4 fiber films (data not shown) reveals a weak pattern, consisting of streaks and lines of spots along a single muscovite direction. This pattern is similar to the ones observed for other *para*-phenylenes. It is characteristic for lying molecules,[3] but it is too weak to be analyzed quantitatively. We conclude that an initial wetting layer from lying molecules is formed as for the case of some other *para*-phenylenes[3,62] and the thiophene-phenylene cooligomer PPTPP.[8]

After excitation with UV light ($\lambda = 365$ nm), the fibers fluoresce in the blue wavelength region. A spectrum is provided in Figure S2 in the supplementary material. Such a structureless spectrum—compared to other plain and functionalized *para*-phenylenes—is often observed for cyano-functionalization.[63,64] A typical fluorescence microscope image (wavelengths $\lambda \gtrsim 420$ nm) is shown in Figure 2(a) and in Figure S1 in the supplementary material. The transition dipole for fluorescence is oriented along the molecules' long axes. This suggests that the fibers consist of molecules lying on the substrate, opposite to upright standing ones formed on SiO_x.[56] The fluorescence intensity along a single fiber can vary considerably. This observation is in line with the changes of morphology, demonstrated in Figure 1. It is unclear, yet, if the variation of fluorescence intensity simply relates to the different amounts of material, or if different CNHP4 orientations with different tilt angles contribute. The integral distribution of fiber orientations in Figure 2(b) suggests a preferred average growth direction. On the whole muscovite surface, two different rotational domains are observed; see Figures S1(b)-S1(d) in the supplementary material. Fiber orientations are spread by ±5° with respect to the average growth direction, often with the angles −5°, 0°, and 5° being preferably selected. This behavior is rather typical for phenylene based small rodlike organic molecules on muscovite mica since they tend to orient with their long molecule axes perpendicular to the grooves and because the orientation of the molecules' long axes is often close to perpendicular to the long fiber axes.[44]

From the difference of the local fiber orientation (θ_{orient}) and the angle for maximum fluorescence (ϕ_{pol}), the distribution of molecule orientations (β_{mol}) within the fibers is deduced, as can be seen in Figure 2(d). The distribution peaks at two values close to $\beta_{mol} = 90°$, meaning that the projection of the long molecule axis onto the substrate is approximately perpendicular to the long fiber axis. In Figure 2(c), the color-coded values of β_{mol} are superimposed on the fluorescence microscope image, and their integral distribution is plotted in Figure 2(d) Since the polarization angles are perpendicular to the muscovite groove direction and thus do not depend on fiber orientation, the values of β_{mol} do, peaking at 85° and 95°. Similar to the growth of the methoxy-functionalized *para*-quaterphenylene MOP4 on muscovite mica, this suggests a substrate-induced chiral organization into single-handed aggregates of both handedness.[62,65] In addition, a clear contribution of fibers with $\beta_{mol} \approx 90°$ is observed. This is also found in Figure 2(c): those different values, rendered as blue, red, and white, are consistently correlated with the three different growth directions ±5° and 0° along the grooves.

Correlation plots provide further insight into the molecule orientations within fibers and on the substrate. The correlation of different quantities extracted from the polarization analysis is illustrated in Figure 3. In addition to Figure 2, these plots demonstrate that the polarization angle is independent of both the local fiber orientation, Figure 3(a), and the orientational angle, Figure 3(b), but that specific fiber orientations correspond to specific values of the orientational angle β_{mol}, Figure 3(c). The within ±5° uniaxial alignment

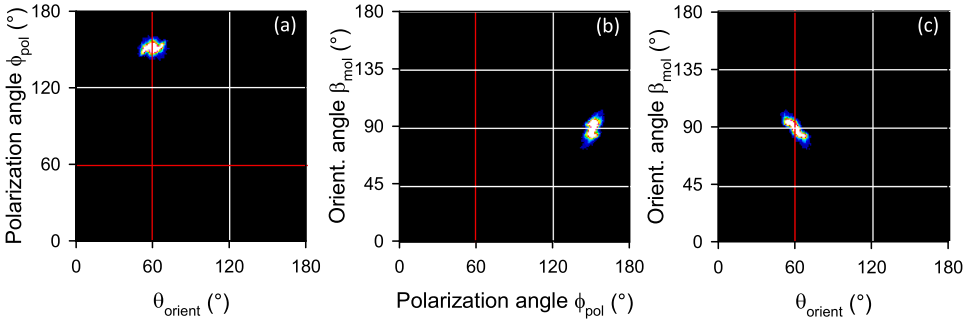

FIG. 3. ((a)-(c)) Correlation plots of polarization angle ϕ_{pol}, fiber orientation θ_{orient}, and molecule orientation β_{mol}, all extracted from polarization dependent fluorescence images of the sample shown in Figure 2(a). Red lines indicate the grooved muscovite direction.

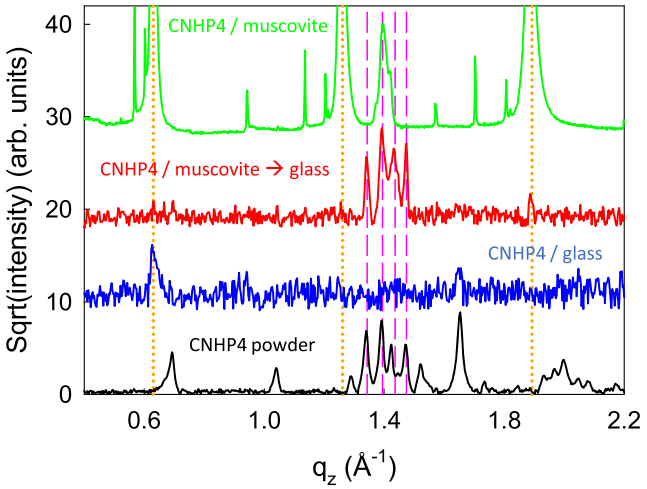

FIG. 4. Specular X-ray diffraction from CNHP4 fibers and thin films. The upper two curves represent diffractograms for CNHP4 fibers still remaining on muscovite mica and wet-transferred onto glass, respectively. Strong muscovite diffraction peaks are designated by vertical, dotted orange lines. Some observed CNHP4 peaks are denoted by vertical pink dashed lines. An X-ray diffractogram of CNHP4 deposited on glass, blue curve, only shows two weak diffraction peaks. A diffractogram from CNHP4 powder is also shown, black lower curve. Except for the case of CNHP4 on muscovite, the glass background has been subtracted.

of the fibers is induced by the *cm* surface symmetry of the muscovite (0 0 1) face, resulting from its dioctahedral nature. For trioctahedral micas with similar lattice constants but no such restricted symmetry like phlogopite and biotite, fibers grow simultaneously along three directions with 60° in between, as detailed in Figures S3 and S4 in the supplementary material.[66]

Contact faces of the fibers with the substrate are determined by X-ray diffraction. Diffractograms are presented in Figure 4 for various CNHP4 samples, all as a function of the component of the scattering vector perpendicular to the substrate surface, $q_z = \frac{4\pi}{\lambda} \sin(2\theta/2)$. Furthermore, X-ray diffraction from CNHP4 powder dispersed on glass is displayed (black lower curve). The powder is assumed to have crystallized in the bulk phase. The upper, green curve in Figure 4, corresponds to diffraction from a thick CNHP4 fiber film of $d = 72$ nm deposited at $T_s = 360$ K, still remaining on muscovite mica. The red curve stems from CNHP4 fibers (grown at a smaller deposition rate and $T_s = 320$ K, $d = 80$ nm) wet-transferred onto glass. The fact that here more diffraction peaks around $q_z = 1.4$ Å^{-1} are visible is due to slightly different deposition conditions. To illustrate that, a comparison of transferred and non-transferred fibers from the same substrate is shown in Figure S5(a) in the supplementary material. Wet-transfer diminishes the muscovite peaks considerably, but does neither disturb the positions of CNHP4 peaks nor induce new ones. This comparison also unmistakeably ensures that the peaks are not related to muscovite mica diffraction peaks, which sometimes are present in the interesting range around $q_z = 1.4$ Å^{-1}, but to different CNHP4 contact faces. CNHP4 deposited on glass (blue curve) does lead to only weak diffraction peaks, where the most prominent one at $q_z \approx 0.62$ Å^{-1} does not directly correspond to any of the peaks observed on mica or for CNHP4 powder. Its position, however, coincides with the one previously observed for the 002 reflection of upright standing CNHP4 molecules formed on SiO_x, on SiO_x treated with octadecyltrichlorsilane (OTS), and on glass.[55,56] Therefore, we conclude that the phase formed on muscovite resembles the CNHP4 bulk phase, and that the previously determined phase of CNHP4 is not forming.

In order to characterize the films more deeply with X-ray diffraction pole figure technique, a large volume of the reciprocal space was mapped.[67] Strong diffraction features were found which could be unambiguously assigned to the 001 orientation of the muscovite single crystal substrate. Characteristic crescent shaped intensities were found at $q = 1.40$ Å^{-1} (with the inclination angles $\Psi = 75°$, 10°, and 0°), at $q = 1.64$ Å^{-1} (with $\Psi = 50°$), and at $q = 1.99$ Å^{-1} (with $\Psi = 20°$ and 90°). The enhanced intensities are marked by ellipses in the corresponding pole figures (Figure 5). These diffraction features are assigned to crystals of CNHP4 since the observed peak positions (q as well as Ψ values) are the characteristic for herringbone packing of rod-like conjugated molecules.[68] Please note that the known CNHP4 polymorph as well as para-quaterphenylene pack in a herringbone fashion. These results allow a rough determination of the orientation of the CNHP4 molecules relative to the substrate surface.

The agreement between X-ray pole figures and optically observed fiber orientations is satisfactory. Both show a spread of fiber orientations of ±5° with respect to the grooved muscovite direction. Optical measurements predict that the long molecule axes for all fiber directions are within ±5°, all parallel to each other and perpendicular to the groove direction, i.e., along [3 1 0] (or [3 $\bar{1}$ 0] for the other groove direction). This leads to an inclination of the long molecule axis by 5° with respect to the fiber direction for the outlier fiber orientations. For these two orientations, the molecular angles are $\beta_{mol} = 85°$ and 95°. These orientations are sketched in the

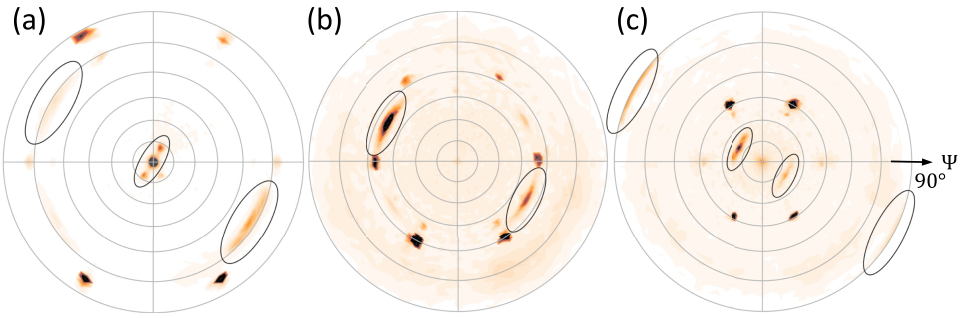

FIG. 5. Pole figures measured at $q = 1.40$ Å^{-1} (a), at $q = 1.64$ Å^{-1} (b), and at $q = 1.99$ Å^{-1} (c). The ellipses give directions of enhanced pole densities which can be unambiguously explained by the epitaxially aligned crystals of the molecule CNHP4. The remaining enhanced pole densities arise from the single crystalline muscovite substrate.

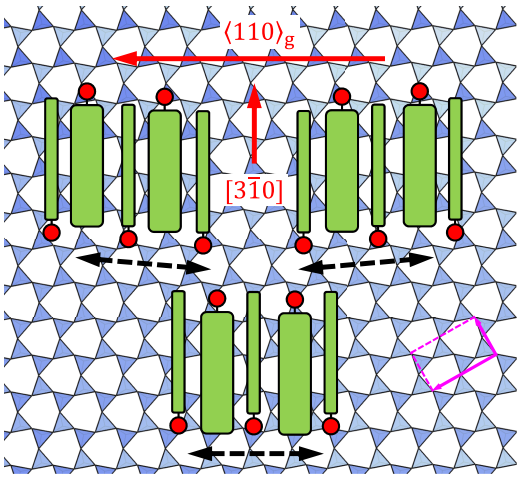

FIG. 6. Proposed schematic orientations of CNHP4 molecules with two mirrored contact faces on muscovite mica (0 0 1),[69] leading to two fiber orientations rotated by ±5° with respect to muscovite $\langle 1\,1\,0\rangle_g$. The long molecule axes are within ±5° parallel to muscovite [3 $\bar{1}$ 0]. In addition a third fiber type is sketched with $\beta_{mol} = 90°$. Red circles mark the nitrogen atoms of CNHP4, and the green box the quaterphenylene tail arranged in a herringbone fashion. Dashed black arrows visualize the proposed fiber directions. The muscovite surface unit cell is denoted by pink solid lines.

upper part of Figure 6. In the phase forming on SiO_x, neighboring molecules are oriented antiparallel with respect to the cyano group. Since the exact arrangement of the molecules within the unit cell is unknown, only a schematic is shown in Figure 6, assuming a herringbone arrangement and antiparallel molecule orientations. The optically determined orientation with $\beta_{mol} = 90°$ is included in the lower part. Obviously, the molecular orientation is induced by the substrate, whereas the aggregation into fibers mainly is determined by intermolecular interactions. Note that the three-dimensional arrangement of the molecules must not show inversion symmetry since CNHP4 nanofibers are able to produce a large amount of second-harmonic radiation after illumination with near-infrared laser pulses.[49]

Since the fibers are at least partially crystalline, their different crystal facets are expected to have unlike surface charges and surface dipoles, which should manifest in different electrostatic properties. To illustrate that, the electric surface potential of the facets is explored by Kelvin probe force microscopy without illumination. As expected, KPFM images of thin and thick CNHP4 fibers samples show noticeable differences in the surface potential of different fiber facets, and between the two fiber types. It can be seen in Figure 7(a) and in the corresponding cross section in Figure 7(b) that for samples of a few nanometers nominal thickness, a clear difference between fibers with well defined faces and the more ill defined ones is present. The surface potential of the ill defined fibers is negative with respect to muscovite mica. It is up to 250 mV more negative than that of the faceted fibers, which is on the other hand more positive than that of muscovite. The side faces of the well defined CNHP4 fibers are often at a higher surface potential than their top. For a number of fibers, one side face is the dominating one—such an asymmetry is also observed in the topography, where different facet slopes emerge. According to Figures 7(c) and (d), thicker CNHP4 samples show a stronger variety of topography as well as of surface potential. Surface potential differences between various parts of the fibers of more than 800 mV are reached. Again, different side faces contribute differently to the surface potential.

Work on the electric surface potential of fibers from the methoxy functionalized quaterphenylene MOP4, mostly condensing into a single fiber morphology, has been performed previously.[70] Merely a negative surface potential with respect to muscovite has been found, with only minor variations along the fibers. On the other hand, a similar bimodal result as for CNHP4 has been obtained for the surface potential of nanofibers from the symmetrically cyano-functionalized quaterphenylene CNP4,[46] where also two different fiber

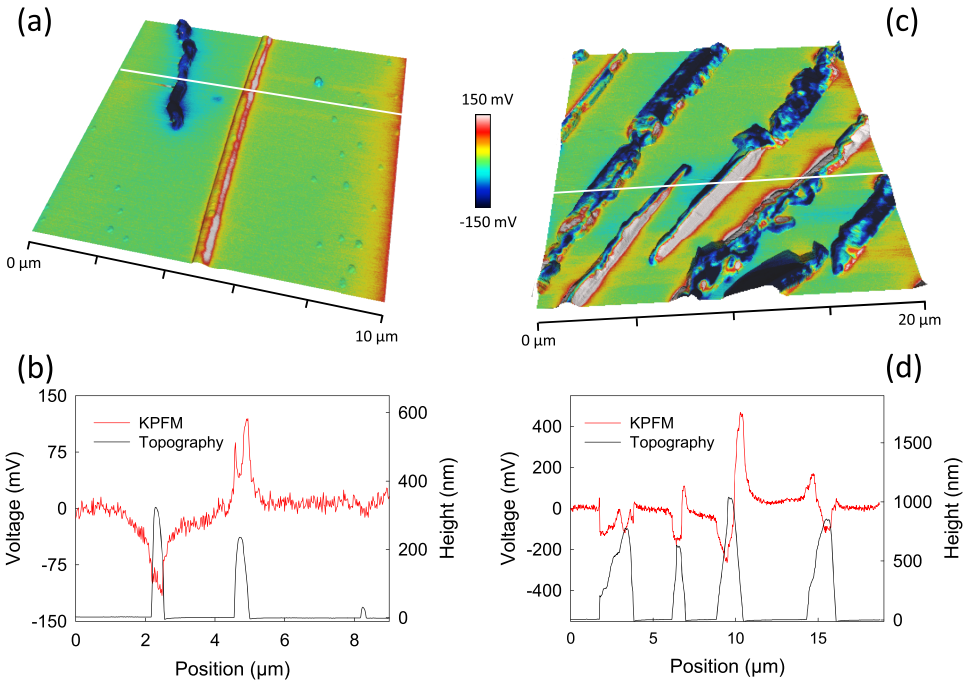

FIG. 7. Three-dimensional views of AFM images of CNHP4 fibers grown on muscovite mica, where the surface potential is superimposed; (a) nominal thickness 8 nm, (c) 83 nm. The surface potential is given with respect to that of muscovite mica. In (b) and (d), cross sections for topography and surface potential are presented for both samples, respectively, marked as white lines in (a) and (c).

morphologies are present on muscovite. For similarly thick films as for CNHP4, the surface potential also differs between side and top faces. This suggests that the electrostatic properties of CNHP4 (and CNP4) fibers are dominated by the strongly electron withdrawing cyano groups. A positive value of the surface potential can be correlated with facets exposing the electron pulling cyano groups. More negative values supposedly stem from facets exposing the phenylene backbone of the CNHP4 molecules.[71–73]

IV. CONCLUSIONS

In this paper, it has been demonstrated that CNHP4 molecules condense into mutual parallel nanofibers after their vacuum deposition on muscovite mica. The long fiber axes evolve along the grooved muscovite direction. Such a growth is rather typical for rodlike phenylenes. On a single muscovite domain, the orientational spread is around 10°. The X-ray diffractogram resembles the bulk crystal structure although a number of different contact faces are found. Two different fiber morphologies are observed, which differ also in the surface potential. However, a clear correlation between the polarization properties, crystal structure, morphology, and surface potential of the fibers is still missing. It demands the determination of the CNHP4 bulk crystal structure as well as the specific contact faces of the different fiber types. Electric surface potentials have been used in the past to monitor, e.g., packing within organic poly(3-hexylthiophene-2,5-diyl) (P3HT) nanofibers, thus discriminating between H- and J-aggregates.[74] Crystal facets with strongly varying surface potentials, which also have been observed previously for, e.g., peptide nanofibers,[75] might contribute to the substantial second harmonic response of such fiber films and might be used in the future to optimize photogeneration for, e.g., organic photodetectors.[76]

SUPPLEMENTARY MATERIAL

See supplementary material for fluorescence spectra of neat and functionalized *para*-phenylenes and for microscopy images of CNHP4 fibers grown on muscovite mica, phlogopite mica, and on biotite. Correlation plots for CNHP4 on biotite are provided, and X-ray diffractograms of as grown and transferred CNHP4 fibers on muscovite and biotite.

ACKNOWLEDGMENTS

Olympus Europa SE & Co. KG, especially J. Mallmann and M. Fabich, is thanked for providing a LEXT OLS4100 confocal laser scanning microscope.

[1] T. Mikami and H. Yanagi, Appl. Phys. Lett. **73**, 563 (1998).
[2] A. Andreev, G. Matt, C. Brabec, H. Sitter, D. Badt, H. Seyringer, and N. S. Sariciftci, Adv. Mater. **12**, 629 (2000).
[3] F. Balzer and H.-G. Rubahn, Surf. Sci. **548**, 170 (2004).
[4] F. Balzer, M. Schiek, A. Osadnik, I. Wallmann, J. Parisi, H.-G. Rubahn, and A. Lützen, Phys. Chem. Chem. Phys. **16**, 5747 (2014).
[5] L. Kankate, F. Balzer, H. Niehus, and H.-G. Rubahn, Thin Solid Films **518**, 130 (2009).
[6] G. Schwabegger, T. Djuric, H. Sitter, R. Resel, and C. Simbrunner, Proc. SPIE **8818**, 88180U (2013).
[7] H. Yanagi, T. Morikawa, S. Hotta, and K. Yase, Adv. Mater. **13**, 313 (2001).
[8] F. Balzer, M. Schiek, A. Lützen, and H.-G. Rubahn, Chem. Mater. **21**, 4759 (2009).
[9] R. Forker, M. Meissner, and T. Fritz, Soft Matter **13**, 1748 (2017).
[10] F. Balzer, V. Bordo, A. Simonsen, and H.-G. Rubahn, Phys. Rev. B **67**, 115408 (2003).
[11] F. Quochi, J. Opt. **12**, 024003 (2010).
[12] H.-H. Fang, J. Yang, J. Feng, T. Yamao, S. Hotta, and H.-B. Sun, Laser Photonics Rev. **8**, 687 (2014).
[13] H. Yanagi, H. Mizuno, F. Sasaki, and S. Hotta, in *Chemical Science of π-Electron Systems* (Springer, 2015), Chap. 38, pp. 635–654.
[14] W. Zhang, J. Yao, and Y. S. Zhao, Acc. Chem. Res. **49**, 1691 (2016).
[15] L. Zang, Y. Che, and J. Moore, Acc. Chem. Res. **41**, 1596 (2008).
[16] M. Wang and B. Gates, Mater. Today **12**, 34 (2009).
[17] F. Kim, G. Ren, and S. Jenekhe, Chem. Mater. **23**, 682 (2011).
[18] M. Schiek, A. Lützen, K. Al-Shamery, F. Balzer, and H.-G. Rubahn, Cryst. Growth Des. **7**, 229 (2007).
[19] R. Resel, T. Haber, O. Lengyel, H. Sitter, F. Balzer, and H.-G. Rubahn, Surf. Interface Anal. **41**, 764 (2009).
[20] I. Wallmann, M. Schiek, R. Koch, and A. Lützen, Synthesis **2008**, 2446.
[21] R. Koch, J. Finnerty, and T. Bruhn, J. Phys. Org. Chem. **21**, 954 (2008).
[22] J. Finnerty and R. Koch, J. Phys. Chem. A **114**, 474 (2010).
[23] P. A. Wood, S. J. Borwick, D. J. Watkin, W. D. S. Motherwell, and F. H. Allen, Acta Crystallogr., Sect. B: Struct. Sci., Cryst. Eng. Mater. **64**, 393 (2008).
[24] F. Klappenberger, D. Kühne, M. Marschall, S. Neppl, W. Krenner, A. Nefedov, T. Strunskus, K. Fink, C. Wöll, S. Klyatskaya, O. Fuhr, M. Ruben, and J. Barth, Adv. Funct. Mater. **21**, 1631 (2011).
[25] S. Gottardi, K. Müller, J. C. Moreno-López, H. Yildirim, U. Meinhardt, M. Kivala, A. Kara, and M. Stöhr, Adv. Mater. Interfaces **1**, 1300025 (2013).
[26] H. Mizuno, T. Maeda, H. Yanagi, H. Katsuki, M. Aresti, F. Quochi, M. Saba, A. Mura, G. Bongiovanni, F. Sasaki, and S. Hotta, Adv. Opt. Mater. **2**, 529 (2014).
[27] W. Hourani, S. Lamare, Y. Makoudi, F. Palmino, and F. Cherioux, Nanotechnology **27**, 425601 (2016).
[28] F. Klappenberger, Prog. Surf. Sci. **89**, 1 (2014).
[29] S. Dokiya, F. Sasaki, S. Hotta, and H. Yanagi, Jpn. J. Appl. Phys., Part 1 **55**, 03DC13 (2016).
[30] K. Torii, S. Dokiya, Y. Tanaka, S. Yoshinaga, and H. Yanagi, "Microneedle crystals of cyano-substituted thiophene/phenylene co-oligomer epitaxially grown on KCl surface," J. Cryst. Growth (in press).
[31] C. Li, M. Hanif, X. Li, S. Zhang, Z. Xie, L. Liu, B. Yang, S. Su, and Y. Ma, J. Mater. Chem. C **4**, 7478 (2016).
[32] G. Koller, S. Berkebile, J. Krenn, G. Tzvetkov, G. Hlawacek, O. Lengyel, F. Netzer, C. Teichert, R. Resel, and M. Ramsey, Adv. Mater. **16**, 2159 (2004).
[33] D. Wrana, M. Kratzer, K. Szajna, M. Nikiel, B. R. Jany, M. Korzekwa, C. Teichert, and F. Krok, J. Phys. Chem. C **119**, 17004 (2015).
[34] T. Djuric, T. Ules, H.-G. Flesch, H. Plank, Q. Shen, C. Teichert, R. Resel, and M. Ramsey, Cryst. Growth Des. **11**, 1015 (2011).
[35] J. Novák, M. Oehzelt, S. Berkebile, M. Koini, T. Ules, G. Koller, T. Haber, R. Resel, and M. G. Ramsey, Phys. Chem. Chem. Phys. **13**, 14675 (2011).
[36] P. Lang, G. Horowitz, P. Valat, F. Garnier, J. Wittmann, and B. Lotz, J. Phys. Chem. B **101**, 8204 (1997).
[37] T. Mizokuro, C. Heck, and N. Tanigaki, J. Phys. Chem. B **116**, 189 (2012).
[38] M. Steinhart, R. Wehrspohn, U. Gösele, and J. Wendorff, Angew. Chem., Int. Ed. **43**, 1334 (2004).
[39] C. Barrett, D. Iacopino, D. O'Carroll, G. De Marzi, D. Tanner, A. Quinn, and G. Redmond, Chem. Mater. **19**, 338 (2007).
[40] K. Bordo, M. Schiek, and H.-G. Rubahn, Appl. Phys. A **114**, 1067 (2014).
[41] N. Uyeda, M. Ashida, and E. Suito, J. Appl. Phys. **36**, 1453 (1965).
[42] S. Kobzareva and G. Distler, J. Cryst. Growth **10**, 269 (1971).
[43] C. Simbrunner, Semicond. Sci. Technol. **28**, 053001 (2013).
[44] F. Balzer and M. Schiek, in *Bottom-Up Self-Organization in Supramolecular Soft Matter*, Springer Series in Materials Science, Vol. 217, edited by S. C. Müller and J. Parisi (Springer, Berlin, 2015), Chap. 7, pp. 151–176.
[45] M. Schiek, F. Balzer, K. Al-Shamery, J. Brewer, A. Lützen, and H.-G. Rubahn, Small **4**, 176 (2008).
[46] F. Balzer, M. Schulz, A. Lützen, and M. Schiek, Soft Matter **12**, 9297 (2016).
[47] J. Brewer, M. Schiek, I. Wallmann, and H.-G. Rubahn, Opt. Commun. **281**, 3892 (2008).
[48] J. Brewer, M. Schiek, and H.-G. Rubahn, Opt. Commun. **283**, 1514 (2010).
[49] K. Pedersen, M. Schiek, J. Rafaelsen, and H.-G. Rubahn, Appl. Phys. B **96**, 821 (2009).

[50]E. Skovsen, T. Søndergaard, J. Fiutowski, P. Simesen, A. Osadnik, A. Lützen, H.-G. Rubahn, S. I. Bozhevolnyi, and K. Pedersen, Opt. Express **20**, 16715 (2012).
[51]T. Leißner, O. Kostiučenko, J. R. Brewer, H.-G. Rubahn, and J. Fiutowski, Appl. Phys. Lett. **107**, 251102 (2015).
[52]J. Iwicki, C. Näther, M. Schiek, A. Lützen, H.-G. Rubahn, W. Krüger, K. Rossnagel, and L. Kipp, Mater. Lett. **63**, 2399 (2009).
[53]T. Yamao, S. Ota, T. Miki, S. Hotta, and R. Azumi, Thin Solid Films **516**, 2527 (2008).
[54]C. Kloc, T. Siegrist, and J. Pflaum, in *Springer Handbook of Crystal Growth* (Springer, 2010), Chap. 25, pp. 845–867.
[55]A. Moser, "Crystal structure determination from two-dimensional powders," Diploma thesis, Graz University of Technology, Graz, 2008.
[56]A. Moser, O. Werzer, H.-G. Flesch, M. Koini, D.-M. Smilgies, D. Nabok, P. Puschnig, C. Ambrosch-Draxl, M. Schiek, H.-G. Rubahn, and R. Resel, Eur. Phys. J.: Spec. Top. **167**, 59 (2009).
[57]F. Balzer and H.-G. Rubahn, Appl. Phys. Lett. **79**, 3860 (2001).
[58]C. Frondel and G. Ashby, Am. Mineral. **22**, 104 (1937).
[59]R. Jahns and F. Lancaster, *Physical Characteristics of Commercial Sheet Muscovite in the Southeastern United States*, Geological Survey Professional Paper 225 (United States Government Printing Office, Washington, 1950).
[60]D. Griffen, *Silicate Crystal Chemistry* (Oxford University Press, New York, 1992).
[61]I. Salzmann and R. Resel, J. Appl. Crystallogr. **37**, 1029 (2004).
[62]F. Balzer, C. Röthel, H.-G. Rubahn, A. Lützen, J. Parisi, R. Resel, and M. Schiek, J. Phys. Chem. C **120**, 7653 (2016).
[63]M. Schiek, F. Balzer, K. Al-Shamery, A. Lützen, and H.-G. Rubahn, Soft Matter **4**, 277 (2008).
[64]Y. Tanaka, K. Goto, K. Yamashita, T. Yamao, S. Hotta, F. Sasaki, and H. Yanagi, Appl. Phys. Lett. **107**, 163303 (2015).
[65]K.-H. Ernst, in *Supramolecular Chirality*, Topics in Current Chemistry (Springer Science + Business Media, 2006), Vol. 265, pp. 209–252.
[66]D. Necas and P. Klapetek, Cent. Eur. J. Phys. **10**, 181 (2012).
[67]R. Resel, O. Lengyel, T. Haber, O. Werzer, W. Hardeman, D. M. de Leeuw, and H. J. Wondergem, J. Appl. Cryst. **40**, 580 (2007).
[68]H. Plank, R. Resel, A. Andreev, N. Sariciftci, and H. Sitter, J. Cryst. Growth **237–239**, 2076 (2002).
[69]K. Momma and F. Izumi, J. Appl. Crystallogr. **44**, 1272 (2011).
[70]F. Balzer, R. Sun, H.-G. Rubahn, M. Schiek, and A. Lützen, Proc. SPIE **8983**, 89830M (2014).
[71]V. Palermo, G. Ridolfi, A. Talarico, L. Favaretto, G. Barbarella, N. Camaioni, and P. Samori, Adv. Funct. Mater. **17**, 472 (2007).
[72]V. Palermo, A. Liscio, M. Palma, M. Surin, R. Lazzaroni, and P. Samorì, Chem. Commun. **2007**, 3326.
[73]*Kelvin Probe Force Microscopy*, Springer Series in Surface Science, Vol. 48, edited by S. Sadewasser and T. Glatzel (Springer, Berlin, 2012).
[74]M. Baghgar and M. D. Barnes, ACS Nano **9**, 7105 (2015).
[75]A. Handelman, G. Shalev, and G. Rosenman, Isr. J. Chem. **55**, 637 (2015).
[76]S. Lee, C.-W. Liang, and L. W. Martin, ACS Nano **5**, 3736 (2011).